Proceedings World Geothermal Congress 2023
Beijing, China, April 17 – 21, 2023

Experimental Investigation on the Dynamic Behaviors and Energy Consumption of Hot Dry Rock under True Triaxial Condition

Hualin Liao[1,*], Jun Wei[1,*], Huajian Wang[1], Zongjie Mu[2,3], Shouceng Tian[2,3], Hongjun Liang[4], Ning Li[4], Hui Yan[4]

(1. School of Petroleum Engineering, China University of Petroleum (East China), Qingdao 266580, China;

2. State Key Laboratory of Petroleum Resources and Exploration, China University of Petroleum-Beijing, Beijing 102249, China;

3. State Key Laboratory of Petroleum Resources and Exploration, China University of Petroleum (Beijing) at Karamay, Karamay 834000, China;

4. Oil and Gas Engineering Research Institute, CNPC Tarim Oilfield Company, Korla 841000, China;)

liaohualin2003@126.com

Keywords: Dynamic behavior; Energy consumption; Hot dry rock; True triaxial stress; Impact damage; Strain rate effect

ABSTRACT

During percussion drilling in deep geothermal reservoir, the high strength of the bottom hole rock (mainly hot dry rock, HDR) resulting from the high three-dimensional in-situ stress leads to a low rate of penetration. Limited by the previously experimental technique, the dynamic behavior and failure mechanism of HDR under dynamic loading and true triaxial stress condition are still unclear. By means of the three-dimensional split Hopkinson pressure bar (3D SHPB) system, the dynamic response of HDR (replaced by granite specimen) is studied. Compared with the traditional Hopkinson device, true triaxial static load can be imposed to a cubic specimen before testing to simulate the confining pressure state in deep well by the 3D SHPB system. The results show that the greater the loading strain rate, the higher the dynamic strength and the greater the energy consumption. Based on the theory of impact damage, the dynamic constitutive model and energy consumption model of rock under impact loads and true triaxial stress condition are established. The dynamic strength and energy consumption of HDR under true triaxial stress have a significantly strain rate correlation, and that express as power function consist with the damage models. The variation laws of elastic parameters of HDR with the strain rate and three-dimensional static stress are analyzed. Combined with the established damage models, the empirical formula for predicting the dynamic energy consumption of HDR in percussive drilling is obtained. This study is helpful for the efficient rock breaking method and theoretical research in deep geothermal reservoir.

1. INTRODUCTION

Due to its good cleanness and reusability, geothermal energy is getting more and more attention. Usually, geothermal energy is deeply buried under 3000-10000 m formation, and mainly distributed in the intersection of several tectonic plates with high geostatic stress, resulting in the bottom hole rock can not be broken effectively. Drilling is an essential step and the only method to explore, develop and utilize the dry hot rock (DHR) resources (Liu & Gao, 2017; Amelia & Paul, 2016), and the percussion drilling method has been proved to significantly improve the bottom hole rock breaking efficiency (Peng et al., 2018; Zhang et al., 2019; Li et al., 2013; Jiang, 2013). However, the dynamic properties of rock under impact loads and three-dimensional stress are unclear now, leading to lack of reference basis for selection of drilling process parameters.

Aiming at the problems of low ROP and serious drill bit wear under high geostatic stress conditions. Smith developed an Axeblade ridged diamond element bit, which reduces the bit surface contact area with the rock, increases the working pressure of a single diamond, and improves drilling efficiency (Due, 2017). The fluidic down-the-hole (DTH) hammer uses the wall effect to realize the reciprocating motion of the piston driving the hammer in the axial direction and transfer the generated impact load to the bit to impact the broken rock. The ROP can be increased by 40.0% to 49.8% in the hard formation. Peng proposed a mathematical model to characterize the wall-attached jet of fluid oscillators and predicted the influence of geometric parameters on critical Reynolds number (Peng et al., 2013), and studied the effect of piston-hammer actuator parameters on the performance of DPOM hammer (Zhang et al., 2016), which increased the ROP to 5.19m/h, which is 3~5 times the conventional method (Zhang et al., 2017).

The dynamic mechanical response of HDR (replaced by the granite specimen) in this paper was studied based on a kind of true triaxial split Hopkinson bar system. And, the dynamic damage constitutive model and energy consumption model were established under the condition of uniaxial impact loads and three-dimensional static prestress. The experimental results and theoretical results were compared showing highly consistency with each other. This study is helpful for the efficient rock breaking method and theoretical research in deep geothermal reservoir.

2. THEORETICAL ANALYSIS

The failure process of rock under dynamic loading is not only related to the amplitude of external load, but also closely related to its acting duration. According to the dynamic damage theory of rock-like materials, as a result of the natural defects and original microcracks inside the rock, the tensile and compressive alternating stress will be generated under the action of dynamic loading, which may lead to the continuously activation and expansion of natural defects and microcracks, causing the accumulation of damage and forming volume fragmentation of the rock finally. Therefore, the damage factor D can be used to characterize the failure status, D=0 indicating there is no damage formed, while D=1 indicating the rock is failured completely. According to the definition of effective stress (Lemaitre, 1983; Zhang et al., 2013), it can be expressed as follows

List Authors in Header, surnames only, e.g. Smith and Tanaka, or Jones et al.

$$\sigma_i = \sigma_i^* \left(1-D\right), \quad \left(i=1,2,3\right) \tag{1}$$

Before the appearance of macro cracks during loading, the strength characteristics have been affected bu the local micro cracks. According to the generalized Hooke's law, the relationship between strength and deformation characteristics of the specimen under three-dimensional static stress in the impact direction is

$$\sigma_1^* = E\varepsilon_1 + \mu\left(\sigma_2^* + \sigma_3^*\right) \tag{2}$$

Combining the above two Eqs to obtain that

$$\begin{cases} \mathrm{d}\sigma_i = \left(1-D\right)\mathrm{d}\sigma_i^* - \sigma_i^*\mathrm{d}D \\ \mathrm{d}\sigma_1^* = E\mathrm{d}\varepsilon_1 + \mu\left(\mathrm{d}\sigma_2^* + \mathrm{d}\sigma_3^*\right) \end{cases} \tag{3}$$

According to Eq(3), the dynamic damage constitutive model of rock under three-dimensional stress and uniaxial impact loading can be obtained as that

$$\mathrm{d}\sigma_1 = E\left(1-D\right)\mathrm{d}\varepsilon_1 + \mu\left(\mathrm{d}\sigma_2 + \mathrm{d}\sigma_3\right) - E\varepsilon_1\mathrm{d}D \tag{4}$$

The key point to analyze the dynamic properties of rock by Eq(4) lies in the determination of the damage factor *D*. Grady (Deng et al.,2016; Grady et al., 1979; Grady et al., 1980) established the damage model of rock at a certain strain rate $\dot{\varepsilon}$ while the action time is *t*, which can be described as

$$D = \alpha\dot{\varepsilon}^m t^{m+3} \tag{5}$$

So that, while the specimen is damaged (*D*=1), the corresponding failure time t_f can be obtained as follows

$$t_f = \alpha^{\frac{-1}{m+3}}\dot{\varepsilon}^{\frac{-m}{m+3}} \tag{6}$$

Utilizing the Hopkinson testing system, under the condition of medium and low strain rate, ignoring the boundary effect of the specimen, the constant strain rate acted on the specimen can be achieved by using the waveform shaping technology (Hu et al., 2019; Nemat, 1991). The relationship between the strain of the specimen in the impact direction and the strain rate is $\mathrm{d}\varepsilon = \dot{\varepsilon}\mathrm{d}t$ And then, the dynamic stress acted on the specimen in the impact direction can be obtained by integrating with Eq(5), shown as below

$$\sigma\left(t\right) = \int \mathrm{d}\sigma_1 = E\dot{\varepsilon}t - \alpha E\dot{\varepsilon}^{m+1}t^{m+4} + \mu\left(\sigma_2 + \sigma_3\right) \tag{7}$$

Therefore, the strain energy absorbed by the specimen can be obtained as below

$$E_s = \int_0^t \sigma\left(t\right)\mathrm{d}\varepsilon = \int_0^t \sigma\left(t\right)\dot{\varepsilon}\mathrm{d}t = \frac{1}{2}E\dot{\varepsilon}t^2 - \frac{\alpha E\dot{\varepsilon}^{m+2}t^{m+5}}{\left(m+5\right)} + \mu\dot{\varepsilon}\left(\sigma_2+\sigma_3\right)t \tag{8}$$

Eq(7) and Eq(8) are the dynamic strength and energy consumption calculation models of rock while it damaged under a certain strain rate. According to the two models, the dynamic strength and energy consumption of rock growth in power with the loading strain rate. As we can know that the stress-strain curve appears an inflection point while the peak stress occurred, and the first derivative must be equal to 0. Hence, the peak stress σ_c under dynamic loading acted on the specimen in the impact direction and the corresponding loading time t_c can be obtained by the first derivative of Eq(7) for time, which can be expressed as follows

$$\sigma_c = E\left(m+3\right)\left(m+4\right)^{-\frac{m+4}{m+3}}\alpha^{\frac{-1}{m+3}}\dot{\varepsilon}^{\frac{3}{m+3}} + \mu\left(\sigma_2+\sigma_3\right) \tag{9}$$

$$t_c = \left(m+4\right)^{\frac{-1}{m+3}}\alpha^{\frac{-1}{m+3}}\dot{\varepsilon}^{\frac{-m}{m+3}} \tag{10}$$

Therefore, it can be further obtained that the energy consumption (E_c and E_f) in the peak stress and while the specimen damaged under three-dimensional stress and uniaxial impact loading are respectively

$$E_c = \frac{E\left(m+3\right)\left(m+6\right)}{2\left(m+5\right)}\left(m+4\right)^{\frac{-m-5}{m+3}}\alpha^{\frac{-2}{m+3}}\dot{\varepsilon}^{\frac{6}{m+3}} + \mu\left(\sigma_2+\sigma_3\right)\left(m+4\right)^{\frac{-1}{m+3}}\alpha^{\frac{-1}{m+3}}\dot{\varepsilon}^{\frac{3}{m+3}} \tag{11}$$

$$E_f = \frac{E(m+3)}{2(m+5)}\alpha^{\frac{-2}{m+3}}\dot{\varepsilon}^{\frac{6}{m+3}} + \mu(\sigma_2+\sigma_3)\alpha^{\frac{-1}{m+3}}\dot{\varepsilon}^{\frac{3}{m+3}} \quad (12)$$

In the above Equations, σ_1, σ_2 and σ_3 indicates the nominal stress of the specimen in three directions; σ_1^*, σ_2^* and σ_3^* indicate the effective stress acted on the specimen in three direction; E indicates the dynamic elastic modulus; μ indicates the Poisson's ratio; D indicates the damage factor under dynamic loading; $\alpha = \frac{8\pi C_g^3 k}{(m+1)(m+2)(m+3)}$, where, k and m are constant to characterize the internal damage activation status of materials; C_g indicates the crack propagation speed inside rock, which is generally considered to be constant, m/s;

3. METHODOLOGY

3.1 Testing Apparatus

The dynamic mechanical responses of HDR were tested utilizing the True Triaxial Split Hopkinson Pressure Bar (3D SHPB) system at the state key laboratory of petroleum resources and exploration, China University of Petroleum (Beijing) at Karamay, China, shown in Figure 1(a). The 3D SHPB system is mainly composed of pneumatic servo control center, striker launching assembly, laser velocimeter, triaxial static loads application system, specimen clamping device, hydraulic station, operation center, signal monitoring and receiving system, etc. The cubic specimen was positioned by 6 steel square bars (X, Y and Z directions) in the clamping device of the 3D SHPB system, as can be seen in Figure 1(b). And, the working principle of the apparatus is shown in Figure 1(c). The striker was launched to impact the incident bar at a certain velocity V_0 along the X-axis, and then, the elastic incident wave (ε_i) was generated and propagate along the incident bar. While the incident wave travelled to the interface of the incident bar and the specimen, part of the incident wave was reflected as a reflected wave (ε_r) to the incident bar due to their impedances mismatch, and part of the incident wave was transmitted as a transmission wave (ε_t) along the impact direction. As a result of the Poisson effect, the corresponding transmission waves (ε_{y1}, ε_{y2}, ε_{z1} and ε_{z2}) generated along the other bars. More details about its working process can be referred to the papers of Xu (Xu et al., 2020; Chen et al., 2014). Compared with the traditional Hopkinson system, the 3D SHPB system adopts six square bars with the section size of 50 mm×50 mm, which are made of finishing machined high-strength steel, and the yield strength after heat treatment shall not less than 1200 MPa. So that, the axially static pre-stress σ_x, σ_y and σ_z can be applied on the cubic specimen by means of the steel bars to simulate the confining pressure states in deep formation, the maximum static load can reach 240 MPa.

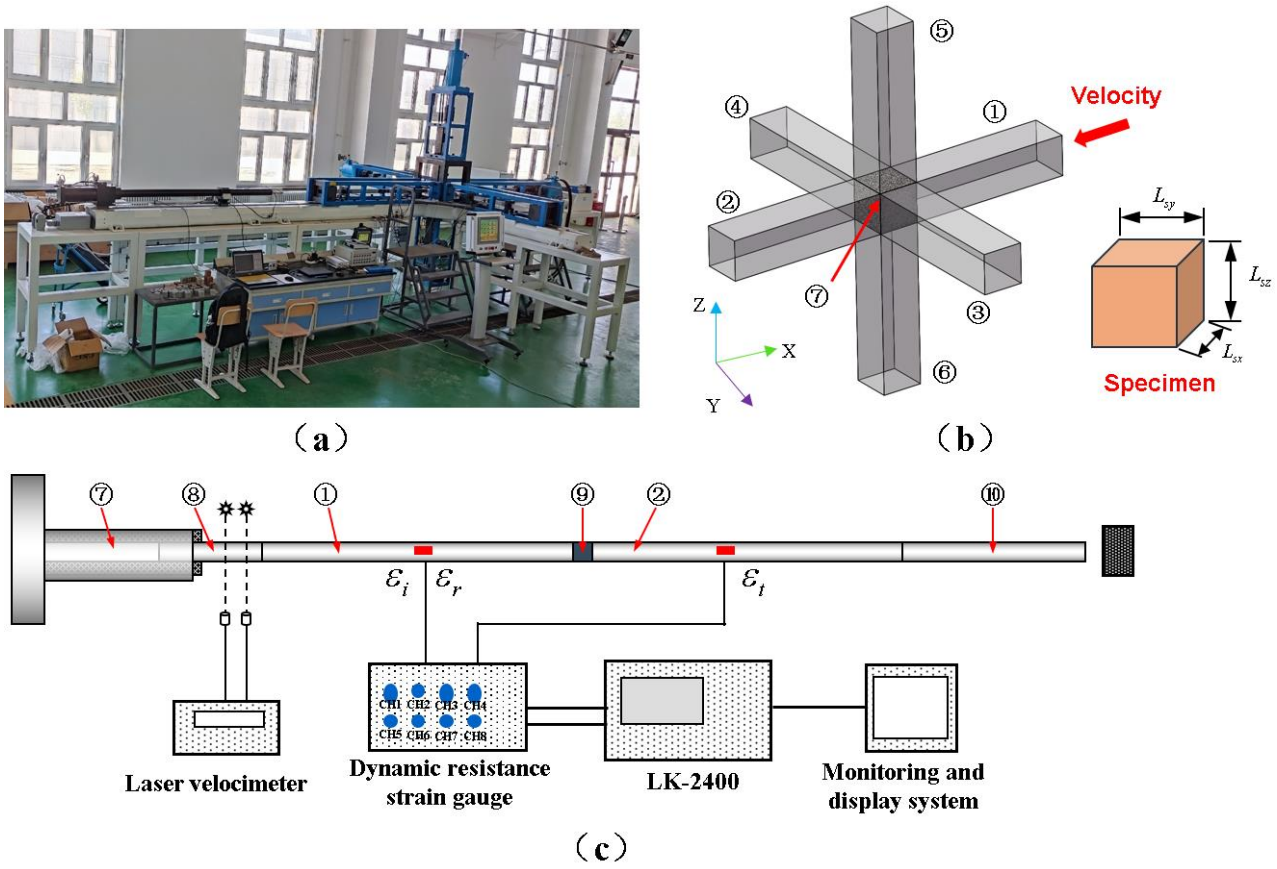

Figure 1: The true triaxial Split Hopkinson Pressure Bar system: (a) 3D SHPB system (b) Clamping device (c) Schematic diagram of SHPB① Incident Bar; ②Transmission Bar; ③Transmission Bar Y1; ④Transmission Bar Y2; ⑤Transmission Bar Z1;⑥ Transmission Bar Z2; ⑦Pneumatic Launcher; ⑧Striker; ⑨Specimen; ⑩Absorber Bar

3.2 Method of Data Processing

The true triaxial dynamic mechanical characteristics can be calculated respectively by measuring the dynamic response signals on the six surfaces of the specimen, monitored by the six square steel bars. Consequently, the key points are to record the dynamic response during impacting. Similar with the conventional SHPB tests, according to the waves measured on each bar, the strain rate $\dot{\varepsilon}_{dx}$, strain ε_{dx} and stress σ_{dx} of the specimen are calculated by the three-wave method (Chen et al., 2014; Li et al., 2018) respectively as follows.

$$\dot{\varepsilon}_{dx}(t)=\frac{C_0}{L_{sx}}\left(\varepsilon_i(t)-\varepsilon_r(t)-\varepsilon_t(t)\right) \tag{13}$$

$$\varepsilon_{dx}(t)=\frac{C_0}{L_{sx}}\int_0^t\left(\varepsilon_i(t)-\varepsilon_r(t)-\varepsilon_t(t)\right)dt \tag{14}$$

$$\sigma_{dx}(t)=\frac{A_0}{2A_{sx}}E_0\left(\varepsilon_i(t)+\varepsilon_r(t)+\varepsilon_t(t)\right) \tag{15}$$

Taking the differences of forces applied on the opposite surface of the specimen into account, the load applied on the specimen was calculated by an average of the two forces. So that, the strain ε_{dj} and stress σ_{dj} (where j indicates the transmission bar in Y-axis and Z-aixs) can be calculated as below.

$$\varepsilon_{dj}(t)=\frac{C_0}{L_{sj}}\int_0^t\left(\varepsilon_{j1}(t)+\varepsilon_{j2}(t)\right)dt \tag{16}$$

$$\sigma_{dj}(t)=\frac{A_0}{2A_{sj}}E_0\left(\varepsilon_{j1}(t)+\varepsilon_{j2}(t)\right) \tag{17}$$

Furthermore, according to the dynamic response signal of each bar, the incident energy E_{in}, reflection energy E_{re} and transmission energy $E_{tr\text{-}j}$ were calculated as

$$E_i=A_{sx}E_0C_0\int_0^\tau\varepsilon_i^2(t)dt \tag{18}$$

$$E_{tr-j}=A_{sj}E_0C_0\int_0^\tau\varepsilon_{tj}^2(t)dt \tag{19}$$

Assuming that the energy loss in the interface between the specimen and the bars is ignored during the impacting, and the ejection kinetic energy of the rock fragment is small enough and can be ignored, the energy absorbed E_A of the specimen during the test is

$$E_A=E_i-E_r-\sum E_{tr-j} \tag{20}$$

Where, A_0 is the cross-sectional area of square bar, E_0 is the Young's modulus of the bars, C_0 is the wave velocity of the bars, L_{sj} represents the size of specimen in j direction, A_{sz} is the cross-sectional area of the specimen.

3.3 Material and Testing Condition

Granite specimens were adopted to represent hot dry rock (HDR) in this study. According to the requirements of the apparatus (the 3D SHPB system), the specimens were processed into cubes with the size of 50 mm × 50 mm × 50 mm, shown in Figure 2. In addition, each face of the specimens had been rounded and polished with elaborate preparation to meet the requirements of ISRM rock mechanics test on the smoothness and parallelism. Where, the parallelism of the three opposite pairs of faces is less than 0.05 mm in 50 mm, the adjacent faces have a good perpendicularity with the maximum deviation of less than 0.25°. The tolerance of the across face is 0.05 mm and the accuracy of the size is kept within ± 1%. Previously, it was obtained by a series of test with the same batch of specimen that the uniaxial compressive strength (UCS) of granite were tested to be about 186.93 MPa, the elastic modulus about 57.9 GPa, and the Poisson's ratio of 0.28.

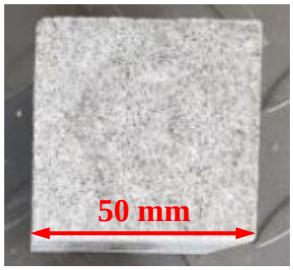

Figure 2 Physical specimen of HDR (replaced by the granite specimen)

To study the dynamic mechanical properties and energy consumption of granite, the initial static pre-stress applied on the specimen was imposed to be triaxial conditions. The initial static confining pressure conditions, marked as [30 MPa, 40 MPa, 50 MPa], were carried out in this study under different dynamic loadings. The experimental scheme is listed in Table 1.

Table 1 The dynamic test scheme

No.	Size/mm			Mass/g	Density ρ/g·cm^{-3}	Impact Velocity /m·s^{-1}	Strain rate/s^{-1}	Static stress/MPa		
	X	Y	Z					σ_x	σ_y	σ_z
THM-04	50.04	50.00	50.06	326.44	2.61	13.16	95.00	30	40	50
THM-12	50.16	50.33	50.04	330.29	2.61	18.18	128.89	30	40	50
THM-14	50.24	50.26	50.21	329.47	2.60	15.39	111.42	30	40	50
THM-15	50.24	50.26	50.21	329.47	2.60	15.87	116.89	30	40	50
THM-16	50.24	50.26	50.21	329.47	2.60	12.20	92.12	30	40	50

It must be mentioned that the initial static pre-stress marked as 0+ refers to the situation of the surface contacting between the bar and the specimen but without any pre-stress applied, so that the impact signals can be captured on the bars to evaluate the dynamic confining stress caused by the Poisson's effect of specimen and the inertial effect of the bar.

The dynamic response signal monitored in the X-axis bars can be seen in Figure 3, while the impact velocity is 13.16 m/s (THM-04), from which we can know that the stress balance conditions ($\varepsilon_i = \varepsilon_t - \varepsilon_r$) are satisfied. Therefore, it can be considered that the dynamic balance realized inner the specimen. It also shows that the 3D SHPB system can be applied to the dynamic of granite, and it can eliminate the transverse inertia effect (Li et al., 2018; Liu et al., 2019).

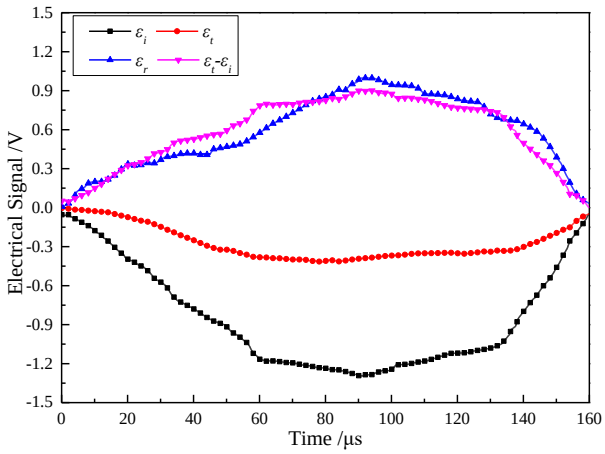

Figure 3 Force balance of the specimen under dynamic load

4. RESULTS AND DISCUSSION

This section refers to the experimental results of granite, which were selected as the substitute for dry hot rock (DHR), so as to discuss the dynamic response and energy consumption of DHR.

4.1 Stress Strain Curves

The relationship between the dynamic stress and strain under different impact velocity can be found in Figure 4, from which we can know that the development trend of curves of dynamic stress and strain of granite changes a lot in the dynamic process. There are a certain of oscillation generated caused by the impact loads. And, due to there is a small difference between each impact velocity of the striker, the dynamic peak stress increase fewer.

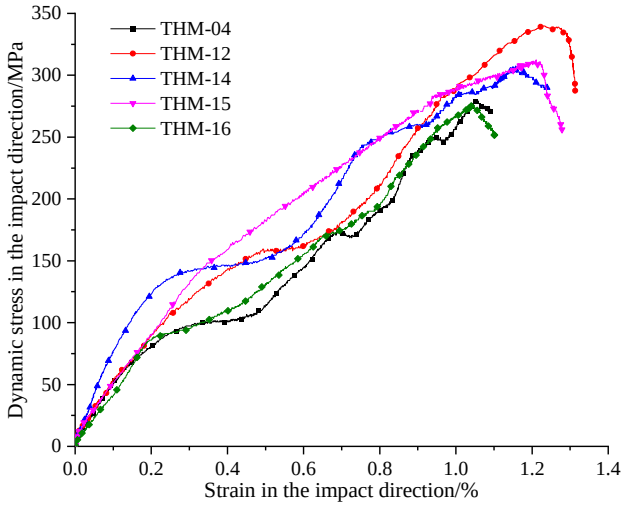

Figure 4 Stress-strain curves under different impact velocity

According to the stress-strain curves above, the dynamic elastic modulus (slope of the stable growth stage of each curve) of these groups of testing specimen can be obtained to be 23.634 GPa (R^2 = 0.9736), 25.276 GPa (R^2 = 0.9718), 23.652 GPa (R^2 = 0.9715), 23.138 GPa (R^2 = 0.9695) and 24.184 GPa (R^2 = 0.9847) respectively, the mean value of which is 23.977 GPa. Where, R^2 indicates the fitting coefficient. The higher fitting coefficient (exceed 0.9695) of the dynamic elastic modulus and the stable relative calculating error (relative to average value, which is lower than 5.42%) show that the impact velocity of striker gives a small effect on the relationship of dynamic stress and strain while it changes in a small range.

4.2 Mechanical parameters

The strain corresponding to the peak stress in the stress-strain curve is called as the failure strain in this paper. According to Figure 4 and the testing results, the peak stress in the three direction were concluded and displayed in Figure 5. Where, the peak stress in each direction were divided into impact strength (X-axis) and the vertical strength (Y-axis and Z-axis), so does the failure strain.

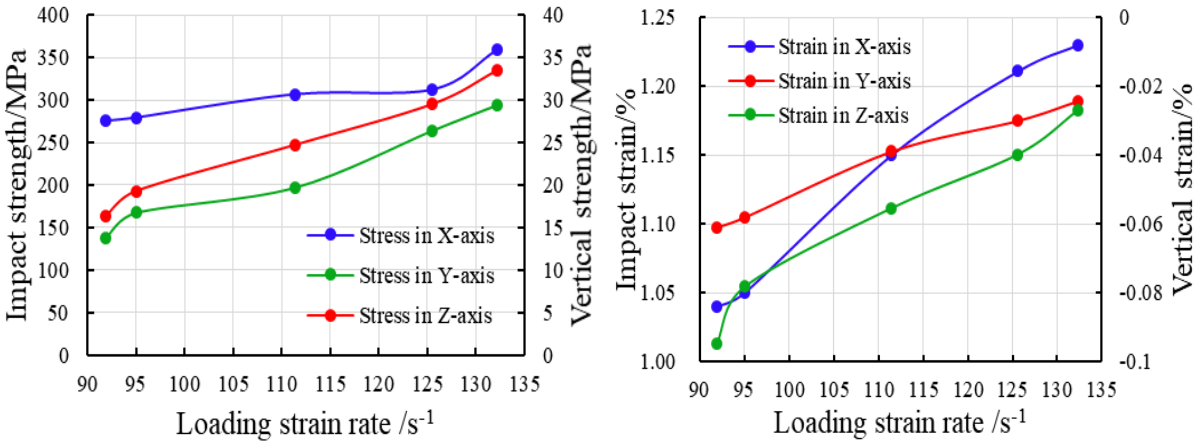

Figure 5 The dynamic strength and deformation characteristics of conglomerate under different strain rates

Figure 5 indicates that the dynamic mechanical properties, mainly the impact strength (also known as the dynamic strength) and the failure strain, of granite are greatly affected by the loading strain rate, and which increases linearly with the impact velocity of the striker (Wei ei at., 2022). Consequently, controlling the vibration characteristics of drill string while drilling appropriately to decrease the strength of bottom hole rock is vital for the rate of penetration. It's worth mentioning that the Heterogeneity of the granite specimen used in the tests were consider to be ignored. So that, the Y-axis and Z-axis of the specimen show the same status in the tests (ignore gravity). Because of the three-dimensional static prestresses applied on the specimens before the tests were 30 MPa, 40MPa and 50 MPa corresponding to X-aixs, Y-axis and Z-axis respectively, the dynamic strength and failure strain in Z-axis are much higher than that in Y-axis, whereas the two parameters in X-axis are significantly higher than the that in the other two directions. The reason for this phenomenon is that the higher the initial static prestress applied on the specimen in a certain direction, the dynamic strength and deformation in that direction could be more obviously caused by the Poisson's effect.

4.3 Energy consumption

According to the dynamic signals monitored in the six bars, the energy acted on the specimen can be obtained so as to analyze its energy consumption characteristics. Based on the Eqs(18)~(21), the energy detected in each bar and the energy absorbed by the testing specimen can be obtained and shown in Table 2.

Table 2 Energy consumption of the specimen

No.	Strain rate /s^{-1}	peak time/μs	E_{in}/J	E_{re}/J	E_{tr_X}/J	E_{tr_Y1}/J	E_{tr_Y2}/J	E_{tr_Z1}/J	E_{tr_Z1}/J	E_A/J	E_V/J·cm^{-3}	E_F/J
THM-04	95.01	139.5	472.30	32.42	233.35	2.27	1.47	3.07	1.18	198.53	1.59	275.98
THM-12	132.27	109.0	392.27	35.70	119.52	1.57	0.03	0.21	0.14	235.10	1.86	326.81
THM-14	111.42	121.9	448.94	22.68	206.79	5.04	0.72	0.63	1.17	211.92	1.67	294.59
THM-15	125.55	123.4	501.79	47.72	234.69	2.99	0.26	0.79	1.73	213.62	1.68	296.95
THM-16	91.87	142.1	554.46	27.62	330.21	3.71	0.59	0.63	1.25	190.45	1.50	264.74

Some scholars have obtained by means of SHPB test that the dynamic strength of rocks-like materials show a power function relationship with the loading strain rate. And, in the situation of middle strain rate (10^1~10^2 s^{-1}) impacting, the exponent of the power function is 1/3 (Li et al., 2015; Li et al., 2017), which indicates that the rock damage constant ***m*** is equal to 6 in Eq(5). Consequently, based on the established rock dynamic damage constitutive model and energy consumption model in section §2, the rock dynamic parameters under middle strain rate rising linearly (***m*** = 6) with second third power of strain rate, and the testing results in Figure 6 confirm this conclusion. Otherwise, the established energy consumption model also shows that the totally energy consumed in the peak stress is 0.72 times with that in the whole loading process.

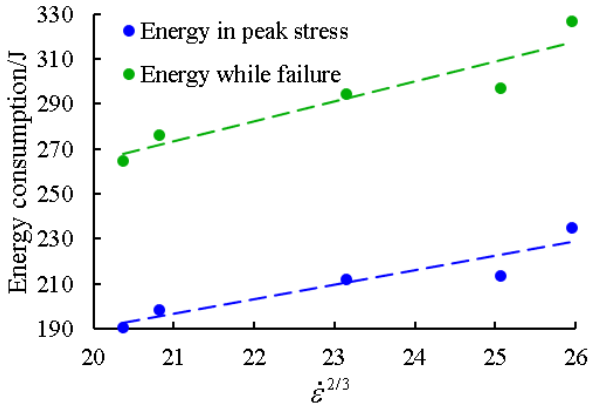

Figure 6 Energy consumption of rock while failure under impact loads

5. CONCLUSIONS

The dynamic damage constitutive model and energy consumption model of rock under uniaxial impact load and true triaxial static prestress condition were established based on damage theory in this paper, and the cubic HDR (replaced by granite specimen) were adopted to carry out the experiments under the same condition utilizing 3D SHPB testing system. The comparison between experimental results and theoretical results shows that the dynamic strength and stress-strain relationship of HDR is related to the loading strain rate, and the energy consumption characteristics of HDR under middle strain rate impact loading condition shows a linearly rising tendency with the second third power of strain rate.

REFERENCES <HEADING 1 STYLE>

Liu W, Gao K. Drilling technical difficulties and dolutions in development of hot dry rock geothermal energy[J]. Advances in Petroleum Exploration and Development, 2017, 13(1):63-69.

Amelia L, Paul S, Stefano S. Performance evaluation of polycrystalline diamond cutter (PDC) bits used in the production interval of well AW-01 in the akiira ranch field, East African Rift Val-ley, Central Kenya[C]. California: Geothermal Resources Council 2016 Annual Meeting, October, 2016.

Peng J, Ge D, Zhang X., et al. Fluidic DTH hammer with backward impact-damping design for hard rock drilling, J. Petrol. Sci. Eng. 2018, 171:1077-1083.

Zhang X, Luo Y, Fan L, Peng J, Yin K, Investigation of RC-DTH air hammer performance using CFD approach with dynamic mesh method, J. Adv. Res. 2019 18: 127-135.

Li G, Suo Z, Wang J. Application of jet hammer and PDC bit in superdeep well[J], China Petrol.2013, 41(4): 31-34.

Jiang R. Simulative experimental research on hydraulic jet hammer applied to superdeep well [J]. Journal of Jilin University (Earth Science Edition), 1990, 20(3): 252 258.

Due Y. Smith bits, A schlumberger company: Axeblade ridged diamond element bit[J]. E & P: A Hart Energy Publication, 2017, 90(5): 83-83.

Peng J, Zhang Q, Li G, et al. Effect of geometric parameters of the bistable fluidic amplifier in the liquid jet hammer on its threshold flow velocity [J]. Computers & Fluids, 2013, 82: 38-49.

Zhang X, Peng J, Ge D, et al. Performance study of a fluidic hammer controlled by an output fed bistable fluidic oscillator[J]. Applied Sciences, 2016, 305: 1-15.

Zhang X, Peng J, Chen J, et al. The effect of actuator parameters on the performance of a liquid jet hammer associated with its jet behavior[J]. Proceedings of the Institution of Mechanical Engineers, Part C: Journal of Mechanical Engineering Science, 2017, 231(14): 2610-2620.

Lemaitre J. How to use damage mechanics[J]. Nuclear Engineering and Design, 1984; 80(3): 233-245.

Zhang M., Wang F., Yang Q. Statistical damage constitutive model for rocks based on triaxial compression tests[J]. Chinese Journal of Geotechnical Engineering, 2013, 35(11): 1965-1971.

Deng Y., Chen M., Jin Y. Investigation of the Dynamic Charecteristics and Energy Consumption for Breaking Rocks Using the Impact Load [J]. PETROLEUM DRILLING TECHNIQUES, 2016, 44(03): 27-32.

Grady D E, Kipp M E. The micromechanics of impact fracture of rock[J]. International Journal of Rock Mechanics and Mining Sciences & Geomechanics Abstracts, 1979, 16 (5): 293-302.

Grady D E, Lipkin J. Criteria for impulsive rock fracture[J]. Geophysical Research Letters, 1980, 7(4): 255–258.

Hu L L, Huang R Y, Gao G F, et al. A novel method for determining strain rate of concrete-like materials in SHPB experiment[J]. Explosion and Shock Waves, 2019, 39(06): 43-51.

Nemat N S. Hopkinson techniques for dynamic recovery experiments[J]. Proceedings of the Royal Society A, 1991, 435(1894): 371-391.

Xu S, Shan J, Zhang L, et al. Dynamic compression behaviors of concrete under true triaxial confinement: An experimental technique[J]. Mechanics of materials, 2020, 140(Jan.):103220.1-103220.18.

Chen X, Wu S, Zhou J. Experimental Study on Dynamic Tensile Strength of Cement Mortar Using Split Hopkinson Pressure Bar Technique[J]. Journal of Materials in Civil Engineering, 2014, 26(6):04014005.

Li X F, Li X, Li H B, et al. Dynamic tensile behaviours of heterogeneous rocks: The grain scale fracturing characteristics on strength and fragmentation[J]. International Journal of Impact Engineering, 2018, 118(AUG.):98-118.

Liu K, Zhang Q B, Wu G, et al. Dynamic Mechanical and Fracture Behaviour of Sandstone Under Multiaxial Loads Using a Triaxial Hopkinson Bar[J]. Rock Mechanics and Rock Engineering, 2019.

Wei J, Liao H L, Wang H J. Experimental investigation on the dynamic tensile characteristics of conglomerate based on 3D SHPB system. Journal of Petroleum Science and Engineering, 2022, 213(3).

Li X B, Lok T S, Zhao J. Dynamic Characteristics of Granite Subjected to Intermediate Loading Rate[J]. Rock Mechanics and Rock Engineering, 2005, 38(1): 21-39.

Li J C, Li N N, Li H B, et al. An SHPB test study on wave propagation across rock masses with different contact area ratios of joint[J]. International Journal of Impact Engineering, 2017, 105:109-116.